Chromosoma (2023) 132:19–29
https://doi.org/10.1007/s00412-023-00785-8

RESEARCH

# Super-resolution microscopy reveals the number and distribution of topoisomerase IIα and CENH3 molecules within barley metaphase chromosomes

**Ivona Kubalová[1] · Klaus Weisshart[2] · Andreas Houben[1] · Veit Schubert[1]**

Received: 30 June 2022 / Revised: 25 October 2022 / Accepted: 13 December 2022 / Published online: 31 January 2023


**Abstract**
Topoisomerase IIα (Topo IIα) and the centromere-specific histone H3 variant CENH3 are key proteins involved in chromatin condensation and centromere determination, respectively. Consequently, they are required for proper chromosome segregation during cell divisions. We combined two super-resolution techniques, structured illumination microscopy (SIM) to co-localize Topo IIα and CENH3, and photoactivated localization microscopy (PALM) to determine their molecule numbers in barley metaphase chromosomes. We detected a dispersed Topo IIα distribution along chromosome arms but an accumulation at centromeres, telomeres, and nucleolus-organizing regions. With a precision of 10-50 nm, we counted ~ 20,000-40,000 Topo IIα molecules per chromosome, 28% of them within the (peri)centromere. With similar precision, we identified ~13,500 CENH3 molecules per centromere where Topo IIα proteins and CENH3-containing chromatin intermingle. In short, we demonstrate PALM as a useful method to count and localize single molecules with high precision within chromosomes. The ultrastructural distribution and the detected amount of Topo IIα and CENH3 are instrumental for a better understanding of their functions during chromatin condensation and centromere determination.

**Keywords** CENH3 · Centromere · Chromatin · *Hordeum vulgare* · Photoactivated localization microscopy · Structured illumination microscopy · Super-resolution · Topoisomerase IIα

## Introduction

Determining the ultrastructures of cell nuclei and chromosomes and quantifying their molecular components are required to understand the dynamics of such basic biological processes as transcription, replication, and cell division. Often, fluorescence dyes are used to label the protein of interest. In contrast to classical fluorescence microscopy techniques, super-resolution microscopy such as structured illumination microscopy (SIM) and single-molecule localization microscopy (SMLM), including photoactivated localization microscopy (PALM) are well suited to achieve ultrastructural imaging by breaking the diffraction limit of light (Schermelleh et al. 2019; Khater et al. 2020). In PALM, fluorophores are excited in such a way that only one molecule of many within the diffraction-limited spot is in its "On" state and can reach precisions up to ~10-40 nm (Betzig et al. 2006).

Meanwhile, SIM, implemented in different microscopic platforms, has been widely used in cell biology (Heintzmann and Huser 2017). It was applied to scrutinize chromosome scaffold proteins (Poonperm et al. 2015) and unveiled the localization of the replication protein A on chromosome axes during meiotic recombination in mammals (Yoon et al. 2018). Moreover, SIM revealed that the mammalian genome, in interphase nuclei, is organized into functional chromatin domains of ~200-300 nm in diameter (Miron et al. 2020).

PALM uncovered dynamic clusters of cohesin and the insulator protein CTCF (Hansen et al. 2017) and contributed to elucidating the mammalian higher-order chromatin structure (Nozaki et al. 2017). PALM was also successfully applied to bacteria to monitor transcription (Stracy and Kapanidis 2017). The development of a three-dimensional (3D) assay for transposase-accessible chromatin-PALM

✉ Veit Schubert
schubertv@ipk-gatersleben.de

[1] Leibniz Institute of Plant Genetics and Crop Plant Research (IPK) Gatersleben, D-06466 Seeland, Germany

[2] Carl Zeiss Microscopy GmbH, D-07745 Jena, Germany

enabled to study chromatin domains and genome topology changes in single cells (Xie et al., 2020).

In plants, SIM was used to visualize chromatin and associated proteins in interphase nuclei and condensed chromosomes (Schubert 2014, 2017; Nemečková et al. 2019; Shi et al., 2019; Zelkowski et al. 2019; Kubalová et al. 2020; Schubert et al. 2020; Municio et al. 2021). Besides, SIM is useful to investigate other cell structures (Schubert 2017) such as microtubules of *Arabidopsis* and *Medicago* (Komis et al. 2014, 2015a, b, 2017, 2018; Vavrdová et al. 2019; Tichá et al. 2020).

On the other hand, SMLM, like PALM studies, is still limited in plants. Schubert and Weisshart (2015) determined the number of RNA polymerase II molecules in differentiated *Arabidopsis* nuclei by PALM. Besides, PALM was used to analyze microtubules and microtubule-associated proteins in *Arabidopsis* root epidermal cells (Vavrdová et al. 2020).

Recently, we compared different super-resolution microscopy methods and proved their superiority over diffraction-limited fluorescence microscopy to analyze chromosomal chromatin. The achieved lateral SIM resolution of ~100 nm and PALM localization precision of up to ~10 nm demonstrated that the combination of both techniques provides a comprehensive overview of Topoisomerase IIα (Topo IIα) localization in barley metaphase chromosomes at the ultrastructural level (Kubalová et al. 2021b).

Topoisomerases are involved in transcription, DNA replication, and chromatin organization (Björkegren and Baranello 2018; Meijering et al. 2022; Pommier et al. 2022). Topo IIα is a dimeric enzyme (~175 kDa in human) owning catalytic and non-catalytic functions. The former depends on ATPase activity, whereas the latter relies solely on the C-terminal domain (CTD) (Fukui and Uchiyama 2007; Edgerton et al. 2016). The catalytic function ensures that supercoiled or catenated DNA becomes resolved via DNA strand passage. Topo IIα introduces double-strand breaks into dsDNA, thus allowing other DNA fibers to pass through. Afterward, the break becomes sealed without any loss of DNA information. This action is important for several biological processes such as DNA replication, transcription, chromosome condensation, and segregation (Nitiss 2009). Although CTD is dispensable for decatenation (Dickey and Osheroff 2005), it is essential for the targeting of Topo IIα in mitotic chromosomes (Lane et al. 2013). First, Topo IIα resolves inter-chromatid entanglements, then it generates intra-chromatid entanglements to promote thickening. Only the latter process requires the CTD (Shintomi and Hirano 2021). The majority of Topo IIα concentrates in the inner centromere and is associated with the control and activation of cell cycle checkpoints as demonstrated in human, mouse, and muntjac cells (Coelho et al. 2008; Lane et al. 2013; Gomez et al. 2013, 2014; Nielsen et al. 2020).

Besides, Topo IIα localizes in chromosome arms. Topo IIα was found as a component of the chicken and human mitotic chromosome scaffolds (Earnshaw and Heck 1985; Earnshaw et al. 1985; Samejima et al. 2012; Chu et al. 2020). The application of light and electron microscopy uncovered twisted double-stranded protein scaffolds in both human metaphase chromatids. These scaffolds are composed of alternating Topo IIα enzymes, condensins, and kinesin family member 4 (KIF4) proteins (Ono et al. 2004; Samejima et al. 2012; Poonperm et al. 2017; Chu et al. 2020). The importance of Topo IIα was demonstrated via its depletion, disrupting the scaffold structure (Poonperm et al. 2015).

Although most data originate from mammalian research, it was reported that plant Topo IIα acts in mitotic and meiotic recombination (Singh et al. 2004). In onion (Zabka et al. 2014) and tobacco (Singh et al. 2017), Topo IIα is involved in cell cycle regulation and removes meiotic bivalent interlocks in *Arabidopsis* (Martinez-Garcia et al. 2018). Thus, Topo IIα possesses several roles while residing on mitotic chromosomes, each requiring a precise location and number of available molecules.

Centromeres, occurring as distinct primary constrictions (monocentromeres) or distributed along chromosomes (holocentromeres) (Schubert et al. 2020), are fundamental for correct chromosome segregation during mitotic and meiotic cell divisions. Thus, they secure the proper distribution of genetic material into daughter cells. Tandemly repeating DNA sequences of different lengths among species are typical for these regions. In contrast to non-centromeric chromatin, most centromeres contain a specific histone H3 variant, termed CENH3 (or CENP-A) (Palmer et al. 1991; Talbert et al. 2002; Cleveland et al. 2003; Ali-Ahmad and Sekulić 2020). In most eukaryotes, CENH3 specifies the position of a proteinaceous complex, the kinetochore, where spindle fibers attach pulling the chromosomes towards both daughter cells (Musacchio and Desai 2017). Vast numbers of proteins residing at the centromere and in the kinetochore detect the fidelity of the spindle fiber attachment and eventually trigger cell cycle checkpoints (Cleveland et al. 2003; Hindriksen et al. 2017). Thus, the vital function of centromeres based on the presence of a certain CENH3 amount is required.

The monocentromeres of most plant species, like rye, barley, *Aegilops speltoides*, and *Cuscuta japonica* are determined by CENH3, and their ultrastructures were analyzed by SIM (Wanner et al. 2015; Schubert et al. 2016, 2020; Oliveira et al. 2020). SIM revealed that barley CENH3 is localized mainly in the interior, rather than at the surface of the monocentromeres. Only a low amount is present in the pericentromeres. Barley encodes two CENH3 variants, αCENH3 and βCENH3, interacting with a fraction of *Cerebra*, a centromeric retroelement

(CR)-like repeat, and besides with a GC-rich centromeric satellite (Houben et al. 2007; Sanei et al. 2011; Schroeder-Reiter et al. 2012). α and βCENH3 colocalize and form together two distinct globular intermingling structures at the primary constriction of mitotic and meiotic metaphase chromosomes (Ishii et al. 2015; Wanner et al. 2015).

SIM has also been used to quantify the relative amount of immuno-labeled CENH3 during the mitotic and meiotic cell cycles of rye (Schubert et al. 2014). However, SIM investigations cannot determine the absolute number of molecules. The specific number and localization of proteins are required to understand their function in the chromatin organization of interphase nuclei and during cell divisions. Moreover, these data are necessary to improve polymer simulations (Câmara et al. 2021; Kubalová et al. 2021a) explaining chromatin condensation along chromosome arms and at centromeres.

In this work, we show that PALM/SMLM is a useful method to count and localize single molecules with high precision. We applied SIM and PALM to localize and quantify the number of Topo IIα and CENH3 molecules based on immuno-labeled somatic barley metaphase chromosomes. The observed accumulation of both proteins within centromeres shows their need to arrange plant centromeres. Furthermore, Topo IIα is present along chromosome arms probably necessary to condense chromatin.

## Results

### Topo IIα occurs dispersed at arms but accumulates at centromeres, telomeres, and NORs of barley metaphase chromosomes

To analyze the distribution of Topo IIα at the ultrastructural level, we stained flow-sorted barley chromosomes with specific antibodies and applied 3D-SIM. Both Topo IIα peptide antibodies raised in rabbits and guinea pigs (Topo IIrb12 and Topo IIgp13, respectively) (Kubalová et al. 2021b) revealed similar enzyme distribution patterns on metaphase chromosomes (Figs. 1, 2; Movies 1, 2). Figure 1 shows the labeling pattern of five different chromosomes. In all of them, Topo IIα occurs in a network-like manner. Movie 1 demonstrates by running through a 3D-SIM image Z stack of the chromosome shown in Fig. 2b that Topo IIα is homogeneously distributed at the surface and within chromosome arms. This becomes also obvious by rotating the same image stack (Movie 2). The satellite chromosomes 5H and 6H (left chromosome in Fig. 1 and bottom chromosome in Fig. 2a) exhibit an accumulation of Topo IIα within their nucleolus organizing regions (NORs). Besides, Topo IIα is accumulated at some telomeres with varying intensity as demonstrated

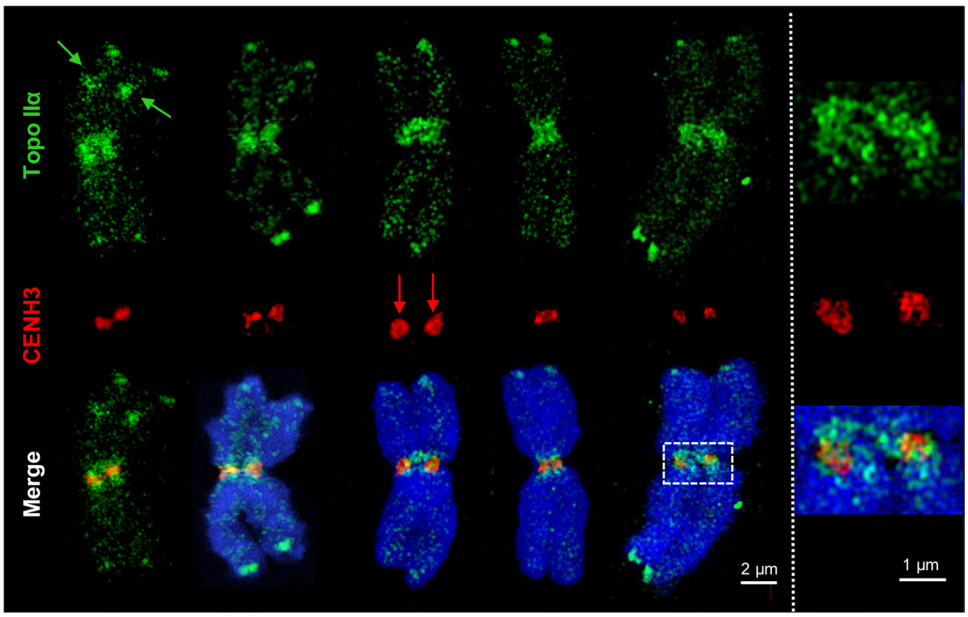


**Fig. 1** Colocalization of topoisomerase IIα (Topo IIα) and CENH3 detected by 3D-SIM. The Topo IIgp13 antibodies used in this experiment show a similar pattern as the Topo IIrb12 antibodies on barley metaphase chromosomes (see Fig. 2). CENH3, sometimes forming ring-like structures (red arrows; Schubert et al. 2016), is embedded within the Topo IIα labeled centromeric chromatin. The satellite chromosome 6H (left) shows Topo IIα labeling also at the NOR regions of both chromatids (green arrows). The telomeres of all chromosomes accumulate Topo IIα with varying intensities. The enlarged pericentromeric region of the right chromosome indicates the intermingling of Topo IIα and CENH3-labeled chromatin. The merge exhibits besides Topo IIα (green) and CENH3 (red) the whole chromosomes stained with DAPI (blue)

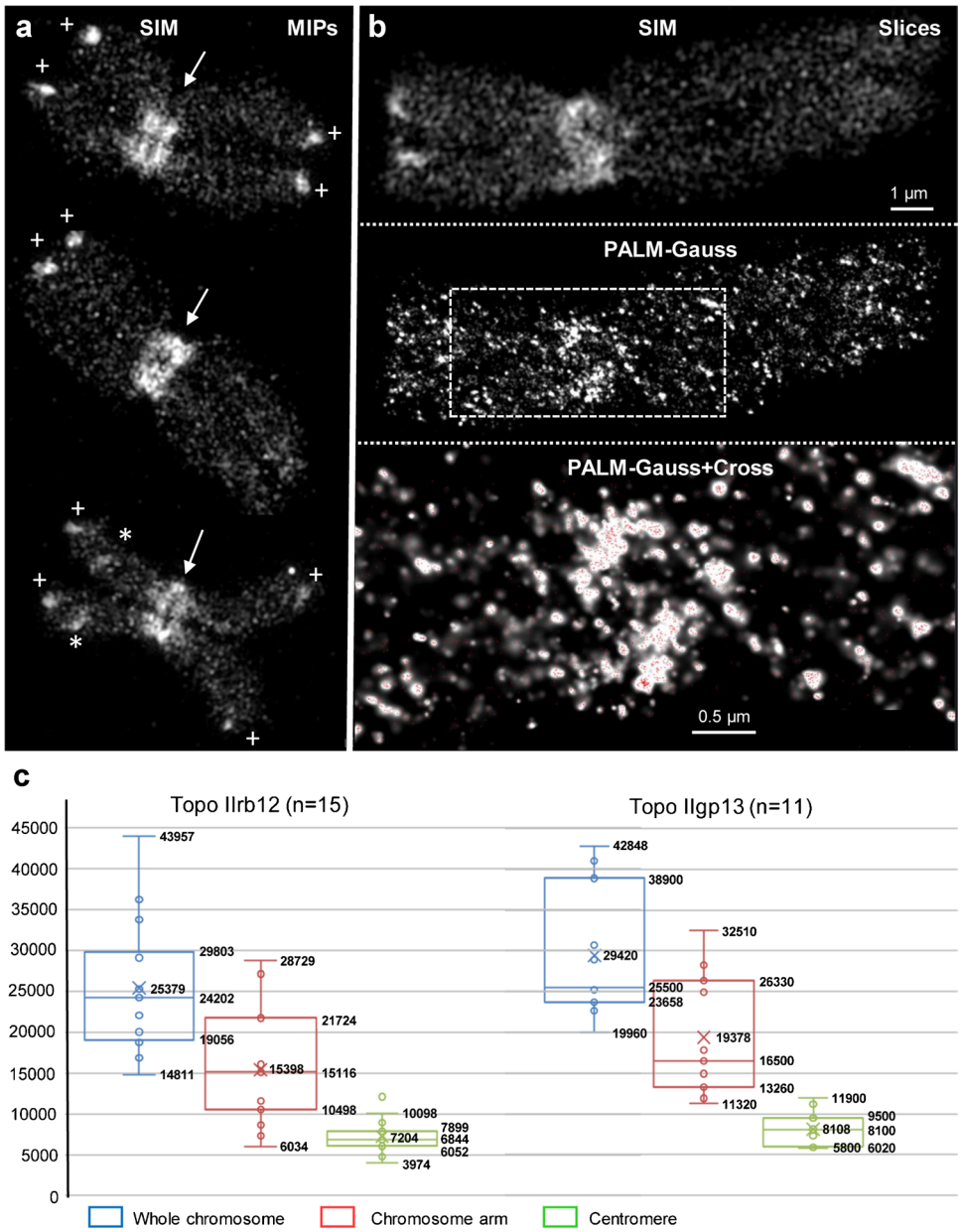


**Fig. 2** 3D-SIM and 3D-PALM of using Topo IIα in different barley metaphase chromosomes visualized by using Topo IIrb12 Alexa488-labeled antibodies. **a** Maximum intensity projections (MIPs) of 3D-SIM image stacks show the accumulation of Topo IIα at all (peri)centromeres (arrows), at some subtelomeres (crosses), and NORs (asterisks) of satellite chromosomes. Topo IIα is homogeneously distributed along all chromosome arms. **b** Single slices of 3D-SIM (top) and 3D-PALM image stacks acquired consecutively from a chromosome showing the Topo IIα accumulation besides at the (peri)centromere only at the short arm telomere. The enlarged region (bottom) within the dashed rectangle of the chromosome visualized via PALM-Gauss (middle) shows additionally the localization of single Topo IIα molecules (red crosses). **c** Boxplots representing the Topo IIα molecule number variability in 15 and 11 chromosomes analyzed by 3D-PALM using Topo IIrb12 and Topo IIgp13 Alexa488-labeled antibodies, respectively. Numbers indicate lower whisker, 25% quantile, median, mean, 75% quantile and upper whisker

especially at the bottom arms of the second and fifth chromosomes. The enzymes concentrate within the pericentromeres as visible on all chromosomes shown in Figs. 1 and 2.

To figure out whether Topo IIα and CENH3-positive chromatin colocalize at centromeres, the chromosomes were labeled with CENH3-specific antibodies in addition (Fig. 1). Similar as shown previously in *Arabidopsis* and cereals (Schubert et al. 2016), CENH3 labels cluster- or ring-like ultrastructures as shown on the third chromosome of Fig. 1. Topo IIα and CENH3 detecting the inner centromere are differently positioned but intermingle among each other (enlarged region of the fifth chromosome in Fig. 1). Movie 3 visualizes the spatial Topo IIα and CENH3 distribution and colocalization in the same rotating 3D-SIM image Z stack.

## Twenty-eight percent of the ~20,000–40,000 Topo IIα molecules per chromosome localize within the pericentromere

To determine the absolute Topo IIα molecule numbers per chromosome, we performed 3D-PALM (Fig. 2b). The PALM imaging confirmed the molecule distribution patterns visualized via SIM. Both different Topo IIα antibodies delivered similar molecule numbers indicating the reliability of the antibodies and the 3D-PALM method.

The chromosome in Fig. 2b showed after 3D-PALM in the Gauss visualization mode a similar Topo IIα distribution as via 3D-SIM. The red crosses within the Gauss mode indicate the exact position of the localized and counted molecules within the enlarged centromeric region of a single PALM slice (Fig. 2 bottom). Running through the PALM-Gauss image Z stack exhibits the spatial distribution of Topo IIα (Movie 4).

The number of Topo IIα molecules (~20,000-40,000) varied highly between the 15 and 11 chromosomes analyzed by Topo IIrb12 and Topo IIgp13 Alexa488-labeled antibodies, respectively (Fig. 2c). On average, ~27,400 Topo IIα molecules are present within whole chromosomes, ~17,400 along arms, and ~7700 around centromeres. That is, ~28% of molecules are accumulated in the (peri)centromeric region (Fig. 2c).

## Topo IIα enzymes surround ~13,500 CENH3-containing nucleosomes at centromeres

To colocalize Topo IIα and CENH3, we immunolabeled flow-sorted barley chromosomes with specific antibodies simultaneously and applied 3D-SIM. While Topo IIα is mainly evident in the pericentromeres, CENH3 concentrates within the core of the primary constrictions and intermingles with Topo IIα-labeled chromatin (Fig. 1; Movie 3). The fluorescence signals of anti-CENH3 were detected only at centromeres, forming one CENH3-positive region per chromatid. Compared to wide-field and deconvolution microscopy, the increased resolution achieved via SIM allowed the detection of looped CENH3-labeled chromatin fibers (Fig. 3a). Besides, CENH3 chromatin may form ring-like structures) (Fig. 1), similar as found in other cereals and *Arabidopsis* (Schubert et al. 2016).

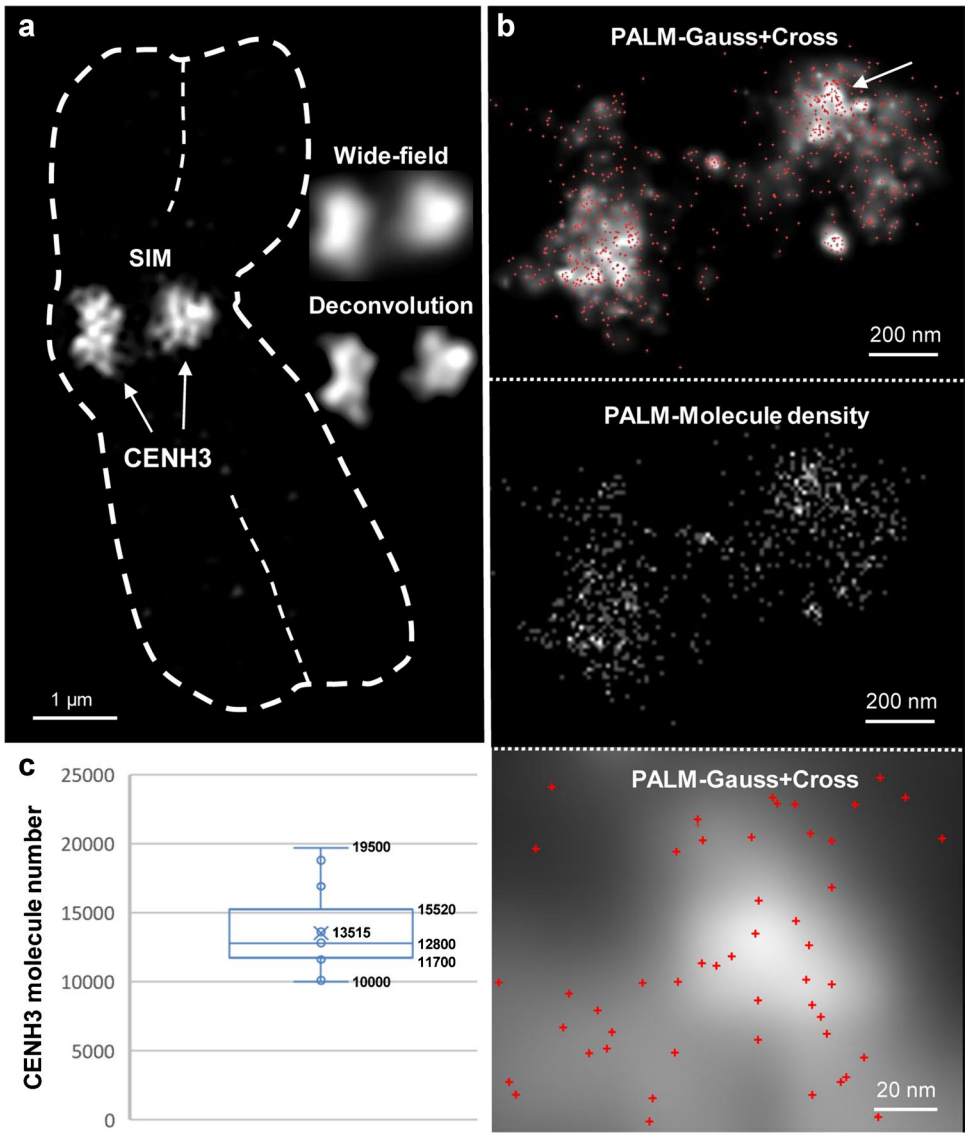


**Fig. 3** 3D-SIM and 3D-PALM of CENH3-containing centromeric chromatin. **a** Both sister centromeres are labeled by CENH3 (arrows) within a barley chromosome (dashed line). SIM increases the resolution compared to widefield and deconvolution microscopy and shows the chromatin ultrastructure. **b** PALM at the same specimen. The "Gauss" and "Molecule density" presentations show the single-molecule distribution in a single slice. The crosses indicate single-molecule positions. The enlarged region (bottom) is indicated (arrow). The axial and lateral molecule localization precisions are shown in Suppl. Fig. 1. **c** Boxplot representing the CENH3 molecule number variability in 13 barley centromeres analyzed by 3D-PALM. Numbers indicate lower whisker (10,000), 25% quantile (11,700), median (12,800), mean (13,515), 75% quantile (15,520), and upper whisker (19,500)

Afterward, 3D-PALM was applied on isolated chromosomes exclusively labeled with CENH3-Alexa488 antibodies (Fig. 3b, c). The labeling pattern was consistent with the SIM imaging. The distinctly localized single molecules (cross presentation) accumulate especially within bright spots of the Gauss display. A mean number of ~13,500 CENH3 molecules per chromosome, i. e., ~6750 per sister centromere, were counted. Compared to Topo IIα, the CENH3 molecule numbers varied less in the 13 barley centromeres analyzed.

3D-PALM allows the detection of single Topo IIα molecules with a lateral (XY) and axial (Z) precision of up to ~10 nm (Kubalová et al., 2021b). We achieved a similar high precision detecting the number of CENH3-containing nucleosomes. About 87% of them were localized laterally and 88% axially with a precision of 10–50 nm (Suppl. Figure 1).

Assuming an octamer structure, each centromeric nucleosome octamer of ~11 nm in diameter contains two CENH3 histones (Nechemia-Arbely et al. 2017). Our achieved PALM localization precision does not allow us to separate both CENH3 histones within a nucleosome. Consequently, each barley metaphase centromere should contain ~27,000 CENH3 molecules.

## Discussion

### 3D-PALM is useful for quantifying single molecules

In this study, we investigated the distribution and the absolute numbers of plant Topo IIα and the centromeric variant of histone H3 (CENH3) in barley metaphase chromosomes. To obtain the numbers and positions of these molecules, we combined two super-resolution microscopic techniques, SIM and PALM. Flow-sorted chromosomes were used because flat and cytoplasm-free specimens can deliver the most informative data. Two different polyclonal peptide antibodies against Topo IIα revealed the localization of this protein with a lateral and axial precisions of ~10-60 nm (Kubalová et al., 2021b). A similar precision we reached for CENH3-specific signals allowing to localize ~88% of single molecules with a distance of ~10-50 nm.

Low numbers of CENH3 molecules were detected in fission yeast with 26 by PALM (Lando et al. 2012), 84 in *Drosophila* using CENH3-EGFP fluorescence intensity measurements (Schittenhelm et al. 2010), and 25-62 in chicken DT-40 cells by SMLM or a confocal microscopy-based fluorescence ratio method (Ribeiro et al. 2010; Johnston et al. 2010). Contrary, in HeLa cells Black et al. (2007) determined at most 30,000 CENH3 molecules, i.e., ~15,000 CENH3-containing nucleosomes per centromere by using immunoblotting of extracts from randomly cycling cells with known amounts of CENH3 as quantitation standards. More recently, Bodor et al. (2014) used an indirect fluorescence method to show that human centromeres contain ~400 CENH3 molecules. This high data variability may be caused by using indirect fluorescence-based molecule counting methods containing possibly erroneous steps.

In our opinion, SMLM with its high precision to localize single molecules is currently the most reliable method to count molecules, albeit limitations apply (Shivanandan et al. 2014). It should be regarded that the number of molecules detected depends on sample integrity, staining efficiency, imaging parameters, and image processing parameters. Consequently, an exact molecule number cannot be provided. Multi-emitter algorithms might be able to single out blinking molecules, but cannot rule out the underestimation of the true molecule number (Dempsey et al. 2011; Oddone et al. 2014).

The amount of ~27,000 CENH3 molecules per centromere we detected in barley is in the range Black et al. (2007) revealed in human chromosomes and is clearly higher than determined by the other above-mentioned authors.

### Topo IIα distribution in barley differs from that in non-plant species

Here, we demonstrate that the most prominent Topo IIα fluorescence signals are present at pericentromeres, NORs of chromosomes 5H and 6H, and some telomeres of mitotic barley metaphase chromosomes. We assume that the telomeric signals of Topo IIα are chromosome-specific because both NOR-bearing chromosomes identifiable after flow-sorting always showed identical Topo IIα-labeling patterns. The high density of Topo IIα in barley pericentromeres and some telomeres is consistent with protein accumulations identified by scanning electron microscopy (Wanner and Schroeder-Reiter 2008).

At barley chromosome arms, Topo IIα is distributed in a reticulate manner. In human HeLa and Chinese hamster cells, Topo IIα, together with condensin, form a line-like protein scaffold inside each chromatid (Maeshima and Laemmli, 2003; Kireeva et al. 2004; Poonperm et al. 2015; Walther et al. 2018). These scaffold proteins were shown to be linked via bridges between the sister chromatids in pig, muntjac, and human (Chu et al. 2020). But it has also been reported that in HeLa cells, the chromatid axes occur as isolated compaction centers rather than forming a continuous line-like scaffold (Sun et al. 2018) and appear to consist of a helical structure that serves to organize chromatin loops into the metaphase chromatid (Phengchat et al. 2019). We suppose that the reticulate scaffold formation in barley may be due to different lengths of major and minor loops forming the 400 nm thick helically organized chromonema building condensed metaphase chromatids. The loop sizes fit experimental Hi-C data induced via a dispersed helical scaffold. Due to the intermingling of ~80 nm lower-order chromatin fibers, the helical chromonema structure is not visible by

3D-SIM on homogeneously stained chromatids but via differential oligo-FISH labeling (Kubalová et al. 2021a).

One Topo IIα enzyme for every 20-50 kb of DNA was estimated to be present in mitotic HeLa metaphase chromosomes (Gasser et al. 1986; Fukui and Uchiyama 2007). In barley chromosome arms, we determined ~27,400 Topo IIα molecules, ~28% of them around centromeres. The genome size of barley containing seven chromosomes is 4.65 Gb DNA (Monat et al. 2019). This corresponds to 664.3 Mb per chromosome. Thus, one molecule of Topo IIα resides at approximately every 24 kb (664.3 Mb /27,400 = 24 kb) of the whole barley chromosome, a value similar to that found for HeLa cells. Due to the accumulation of Topo IIα (~7,700 molecules) in the barley pericentromeres spanning ~100 Mb DNA (Monat et al. 2019), we assume one molecule per 13 kb (100 Mb/7700 =13 kb), and along chromosome arms a lower density with one molecule every 32.5 kb (564.3 Mb/17,400=32.5 kb).

Besides the detection of the accumulation of Topo IIα in pericentromers, NORs and telomeres, and a less prominent amount along chromosome arms, PALM revealed the clustering of Topo IIα in these regions, possibly representing chromatin fiber looping centers. Given the role of Topo IIα in chromosome condensation and its reticular distribution along the chromosomal arms, it would be of interest to apply PALM to condensins, the key components in chromosome organization (Hirano 2012). Walther et al. (2018) detected by fluorescence correlation spectroscopy ~195,000 condensin I and ~35,000 condensin II complexes in HeLa chromosomes. Determining the number and distribution of condensins also in barley chromosomes would improve the understanding of the mitotic condensation process.

### Topo IIα and CENH3 are part of the (peri)centromeric chromatin

Besides epigenetic DNA and histone modifications (Vos et al. 2006; Gieni et al. 2008; Achrem et al. 2020), cohesin, condensin, and SMC5/6 complexes, the main components to organize (peri)centromeres are Topo IIα and CENH3 (Wang et al. 2010; Gomez et al. 2013, 2014; Lawrimore and Bloom 2019a, b). Like in yeast and frog (Ryu et al. 2015; Edgerton et al. 2016; Yoshida et al. 2016; Zhang et al. 2020), barley Topo IIα localizes to the centromeres of metaphase chromosomes.

A positive correlation exists between kinetochore and chromosome size, and the adequate number of attached microtubule spindle fibers are important for correct chromosome segregation during cell division. Larger chromosomes require more microtubules, and thus larger kinetochores to move them with the same velocity as small ones (Nicklas 1965; Plačková et al. 2022). The microtubule-binding capacity increases with kinetochore size in Indian muntjac chromosomes (Drpic et al. 2018) and in rat-kangaroo PtK1 cells, and it was demonstrated that the chromosome size determines the number of microtubules (McEwen et al. 1998). In grass species, the anti-CENH3 signal size is strongly correlated with genome size. Species with large genomes and few chromosomes have the largest centromeres (e.g., rye), while species with small genomes and many chromosomes have the smallest centromeres (e.g., rice) (Zhang and Dawe 2012). Although not as obvious as between species, a positive correlation between kinetochore size and chromosome size was also observed in human (Irvine et al. 2004) and maize (Wang et al. 2021), and within bimodal karyotypes as demonstrated for *Agavoideae* species (Plačková et al. 2022).

We determined ~27,000 CENH3 molecules per centromere for the relatively large barley chromosomes. For comparison, it will be interesting to elucidate the CENH3 amount in small chromosomes by PALM/SMLM.

## Materials and methods

### Plant material, chromosome isolation, and specimen preparation

Barley metaphase chromosomes (*Hordeum vulgare* L. cv. Morex) were sorted according to Lysák et al. (1999). Briefly, a chromosome suspension was prepared from synchronized primary roots meristems. Chromosomes were DAPI-stained, immediately analyzed, and flow-sorted using a FACSAria II SORP flow cytometer and sorter (BD Bioscience, San Jose, CA, USA). Five thousand chromosomes were sorted into 15 µl of PRINS buffer supplemented with 2.5% sucrose (10 mM TRIS, 50 mM KCl, 2 mM $MgCl_2.6H_2O$, 2.5% sucrose; pH 8) onto high precision coverslips (Paul Marienfeld GmbH & Co. KG, Lauda-Königshofen, Germany). Before immunolabeling, the coverslips were stored at −20 °C.

### Indirect immunostaining

Before immunolabeling, coverslips were washed twice with 1×PBS for 5 min at room temperature (RT) and incubated with blocking solution (5% BSA, 0.03% Triton X-100, 1×PBS) for 1.5 h at RT. Peptide Topo IIα (rb12 and gp13) (Kubalová et al. 2021b) and rabbit anti-grassCENH3 (Nagaki et al. 2004; Houben et al. 2007) antibodies were diluted 1:100 and 1:10,000, respectively, in antibody solution (1% BSA, 0.01% Triton X-100, 1 × PBS), and incubated overnight at 4 °C. Grass-CENH3 antibodies detect both α and βCENH3 of barley (Ishii et al. 2015).

Next, coverslips were washed with 1×PBS (three times, 5 min each) at RT and incubated with secondary donkey anti-rabbit Alexa488 (1:200, #711-545-152 Jackson ImmunoResearch) and goat anti-guinea pig Alexa488 (1:200, # A11073 Invitrogen) antibodies for 1 h at 37 °C. For colocalization with Topo IIα, CENH3 was labeled with Cy3-conjugated

anti-rabbit IgG (Dianova). Subsequently, coverslips were washed in 1×PBS (three times, 5 min each) at RT and immediately dehydrated in an ethanol series (70%, 85%, and 100%), each step 2 min. Afterward, the coverslips were air-dried and subjected to microscopy.

## Microscopy

The fluorescence signals of Topo IIα and CENH3 were imaged by wide-field (WF), deconvolution (DCV) of WF, and super-resolution 3D-SIM, using an Elyra PS.1 microscope system equipped with a 63×/1.4 Oil Plan-Apochromat objective and the software ZENBlack (Carl Zeiss GmbH). Images were captured separately for DAPI and Alexa488 using 405 nm and 488 lasers for excitation and appropriate emission filters. Reconstruction of SIM images was done with the ZENBlack software structured illumination processing module. 3D-PALM was performed with the 488 laser and the images were processed with the ZENBlack software PALM processing module. The localization precision in 3D-PALM was calculated via simulations of the experimental point-spread function (Weisshart et al. 2016; Kubalová et al. 2021b). The localization precision is the standard deviation of the data fit. Therefore, it describes the certainty of the localized position or likewise the area within which the molecule is positioned with high likelihood. Determining the resolution is not straightforward and would require the spacing of the labeled molecules. If the spacing of molecules is at least twice as fine as the localization precision, the latter represents according to the Nyquist criterion the resolution. Otherwise, the resolution is twice the spacing. As spacing normally is not known, one has to resort to taking the profile between two structures as described in Kubalová et al. (2021b) to determine the resolution at a specific site. The resolution can be quite different in various areas of the image.

3D rendering of SIM and PALM image stacks to produce movies was performed with the Imaris 9.7 software (Bitplane).

**Supplementary Information** The online version contains supplementary material available at https://doi.org/10.1007/s00412-023-00785-8.

**Acknowledgements** We thank Petr Cápal (Olomouc, Czech Republic) for the flow-sorting of chromosomes and Ingo Schubert for critical reading of the manuscript.

**Author contribution** VS and IK designed the work. IK performed slide preparations. AH provided the CENH3 antibodies. VS performed microscopy. VS and KW analyzed the data. VS and IK wrote the main manuscript text. All authors reviewed the manuscript.

**Funding** Open Access funding enabled and organized by Projekt DEAL. This work was supported by the Deutsche Forschungsgemeinschaft (Schu 762/11-1). Costs for open access publishing were partially funded by the Deutsche Forschungsgemeinschaft (DFG, German Research Foundation, grant 491250510).

**Data availability** There are no additional data and material available.

## Declarations

**Ethics approval** No humans or animals involved to collect research data.

**Conflict of interest** The authors declare no competing interests.



## References

Achrem M, Szucko I, Kalinka A (2020) The epigenetic regulation of centromeres and telomeres in plants and animals. Comp Cytogenet 14:265–311

Ali-Ahmad A, Sekulić N (2020) CENP-A nucleosome-a chromatin-embedded pedestal for the centromere: lessons learned from structural biology. Essays Biochem 64:205–221

Betzig E, Patterson GH, Sougrat R, Lindwasser OW, Olenych S, Bonifacino JS, Davidson MW, Lippincott-Schwartz J, Hess HF (2006) Imaging intracellular fluorescent proteins at nanometer resolution. Science 313:1642–1645

Björkegren C, Baranello L (2018) DNA supercoiling, topoisomerases, and cohesin: partners in regulating chromatin architecture? Int J Mol Sci 19:884

Black BE, Jansen LE, Maddox PS, Foltz DR, Desai AB, Shah JV, Cleveland DW (2007) Centromere identity maintained by nucleosomes assembled with histone H3 containing the CENP-A targeting domain. Mol Cell 25:309–322

Bodor DL, Mata JF, Sergeev M, David AF, Salimian KJ, Panchenko T, Cleveland DW, Black BE, Shah JV, Jansen LE (2014) The quantitative architecture of centromeric chromatin. Elife 3:e02137

Câmara AS, Schubert V, Mascher M, Houben A (2021) A simple model explains the cell cycle-dependent assembly of centromeric nucleosomes in holocentric species. Nucleic Acids Res 49:9053–9065

Chu L, Liang Z, Mukhina M, Fisher J, Vincenten N, Zhang Z, Hutchinson J, Zickler D, Kleckner N (2020) The 3D topography of mitotic chromosomes. Mol Cell 79:902–916 e906

Cleveland DW, Mao Y, Sullivan KF (2003) Centromeres and kinetochores: from epigenetics to mitotic checkpoint signaling. Cell 112:407–421

Coelho PA, Queiroz-Machado J, Carmo AM, Moutinho-Pereira S, Maiato H, Sunkel CE (2008) Dual role of topoisomerase II in centromere resolution and aurora B activity. PLoS Biol 6:e207

Dempsey GT, Vaughan JC, Chen KH, Bates M, Zhuang X (2011) Evaluation of fluorophores for optimal performance in localization-based super-resolution imaging. Nat Methods 8:1027–1036

Dickey JS, Osheroff N (2005) Impact of the C-terminal domain of topoisomerase IIα on the DNA cleavage activity of the human enzyme. Biochemistry 44:11546–11554

Drpic D, Almeida AC, Aguiar P, Renda F, Damas J, Lewin HA, Larkin DM, Khodjakov A, Maiato H (2018) Chromosome segregation is biased by kinetochore size. Curr Biol 28(1344-1356):e1345

Earnshaw WC, Heck MM (1985) Localization of topoisomerase II in mitotic chromosomes. J Cell Biol 100:1716–1725

Earnshaw WC, Halligan B, Cooke CA, Heck MM, αLiu LF (1985) Topoisomerase II is a structural component of mitotic chromosome scaffolds. J Cell Biol 100: 1706-1715.

Edgerton H, Johansson M, Keifenheim D, Mukherjee S, Chacon JM, Bachant J, Gardner MK, Clarke DJ (2016) A noncatalytic function of the topoisomerase II CTD in Aurora B recruitment to inner centromeres during mitosis. J Cell Biol 213:651–664

Fukui K, Uchiyama S (2007) Chromosome protein framework from proteome analysis of isolated human metaphase chromosomes. Chem Rec 7:230–237

Gasser SM, Laroche T, Falquet J, Boy de la Tour E, Laemmli UK (1986) Metaphase chromosome structure. Involvement of topoisomerase II. J Mol Biol 188:613–629

Gieni RS, Chan GK, Hendzel MJ (2008) Epigenetics regulate centromere formation and kinetochore function. J Cell Biochem 104:2027–2039

Gomez R, Jordan PW, Viera A, Alsheimer M, Fukuda T, Jessberger R et al (2013) Dynamic localization of SMC5/6 complex proteins during mammalian meiosis and mitosis suggests functions in distinct chromosome processes. J Cell Sci 126:4239–4252

Gomez R, Viera A, Berenguer I, Llano E, Pendas AM, Barbero JL, Kikuchi A, Suja JA (2014) Cohesin removal precedes topoisomerase IIα-dependent decatenation at centromeres in male mammalian meiosis II. Chromosoma 123:129–146

Hansen AS, Pustova I, Cattoglio C, Tjian R, Darzacq X (2017) CTCF and cohesin regulate chromatin loop stability with distinct dynamics. Elife 6:e25776

Heintzmann R, Huser T (2017) Super-resolution structured illumination microscopy. Chem Rev 117:13890–13908

Hindriksen S, Lens SMA, Hadders MA (2017) The ins and outs of Aurora B inner centromere localization. Front Cell Dev Biol 5:112

Hirano T (2012) Condensins: universal organizers of chromosomes with diverse functions. Genes Dev 26:1659–1678

Houben A, Schroeder-Reiter E, Nagaki K, Nasuda S, Wanner G, Murata M, Endo TR (2007) CENH3 interacts with the centromeric retrotransposon cereba and GC-rich satellites and locates to centromeric substructures in barley. Chromosoma 116:275–283

Irvine DV, Amor DJ, Perry J, Sirvent N, Pedeutour F, Choo KHA, Saffery R (2004) Chromosome size and origin as determinants of the level of CENP-A incorporation into human centromeres. Chromosom Res 12:805–815

Ishii T, Karimi-Ashtiyani R, Banaei-Moghaddam AM, Schubert V, Fuchs J, Houben A (2015) The differential loading of two barley CENH3 variants into distinct centromeric substructures is cell type- and development-specific. Chromosom Res 23:277–284

Johnston K, Joglekar A, Hori T, Suzuki A, Fukagawa T, Salmon ED (2010) Vertebrate kinetochore protein architecture: protein copy number. J Cell Biol 189:937–943

Khater IM, Nabi IR, Hamarneh G (2020) A review of super-resolution single-molecule localization microscopy cluster analysis and quantification methods. Patterns (N Y) 1:100038

Kireeva N, Lakonishok M, Kireev I, Hirano T, Belmont AS (2004) Visualization of early chromosome condensation: a hierarchical folding, axial glue model of chromosome structure. J Cell Biol 166:775–785

Komis G, Mistrik M, Samajová O, Doskočilová A, Ovečka M, Illés P, Bartek J, Samaj J (2014) Dynamics and organization of cortical microtubules as revealed by superresolution structured illumination microscopy. Plant Physiol 165:129–148

Komis G, Mistrik M, Šamajová O, Ovečka M, Bartek J, Šamaj J (2015a) Superresolution live imaging of plant cells using structured illumination microscopy. Nat Protoc 10:1248–1263

Komis G, Samajova O, Ovecka M, Samaj J (2015b) Super-resolution microscopy in plant cell imaging. Trends Plant Sci 20:834–843

Komis G, Luptovčiak I, Ovečka M, Samakovli D, Šamajová O, Šamaj J (2017) Katanin effects on dynamics of cortical microtubules and mitotic arrays in *Arabidopsis thaliana* revealed by advanced live-cell imaging. Front Plant Sci 8:866

Komis G, Novak D, Ovecka M, Samajova O, Samaj J (2018) Advances in imaging plant cell dynamics. Plant Physiol 176:80–93

Kubalová I, Schmidt Černohorská M, Huranová M, Weisshart K, Houben A, Schubert V (2020) Prospects and limitations of expansion microscopy in chromatin ultrastructure determination. Chromosom Res 28:355–368

Kubalová I, Câmara AS, Cápal P, Beseda T, Rouillard J-M, Krause GM, Toegelová H, Himmelbach A, Stein N, Houben A, Doležel J, Mascher M, Šimková S, Schubert V (2021a) Helical metaphase chromatid coiling is conserved. bioRxiv preprint. https://doi.org/10.1101/2021.09.16.460607

Kubalová I, Němečková A, Weisshart K, Hřibová E, Schubert V (2021b) Comparing super-resolution microscopy techniques to analyze chromosomes. Int J Mol Sci 22:1903

Lando D, Endesfelder U, Berger H, Subramanian L, Dunne PD, McColl J, Klenerman D, Carr AM, Sauer M, Allshire RC, Heilemann M, Laue ED (2012) Quantitative single-molecule microscopy reveals that CENP-A(Cnp1) deposition occurs during G2 in fission yeast. Open Biol 2:120078

Lane AB, Gimenez-Abian JF, Clarke DJ (2013) A novel chromatin tether domain controls topoisomerase IIα dynamics and mitotic chromosome formation. J Cell Biol 203:471–486

Lawrimore CJ, Bloom K (2019a) Common features of the pericentromere and nucleolus. Genes (Basel) 10

Lawrimore J, Bloom K (2019b) The regulation of chromosome segregation via centromere loops. Crit Rev Biochem Mol Biol 54:352–370

Lysák MA, Číuhalíková J, Kubaláková M, Šimková H, Künzel G, Doležel J (1999) Flow karyotyping and sorting of mitotic chromosomes of barley (*Hordeum vulgare* L.). Chromosom Res 7:431–444

Maeshima K, Laemmli UK (2003) A two-step scaffolding model for mitotic chromosome assembly. Dev Cell 4:467–480

Martinez-Garcia M, Schubert V, Osman K, Darbyshire A, Sanchez-Moran E, Franklin FCH (2018) TOPII and chromosome movement help remove interlocks between entangled chromosomes during meiosis. J Cell Biol 217:4070–4079

McEwen BF, Ding Y, Heagle AB (1998) Relevance of kinetochore size and microtubule-binding capacity for stable chromosome attachment during mitosis in PtK1 cells. Chromosom Res 6:123–132

Meijering AEC, Sarlos K, Nielsen CF, Witt H, Harju J, Kerklingh E, Haasnoot GH, Bizard AH, Heller I, Broedersz CP et al (2022) Nonlinear mechanics of human mitotic chromosomes. Nature 605:545–550

Miron E, Oldenkamp R, Brown JM, Pinto DMS, Xu CS, Faria AR, Shaban HA, Rhodes JDP, Innocent C, de Ornellas S, Hess HF, Buckle V, Schermelleh L (2020) Chromatin arranges in chains of mesoscale domains with nanoscale functional topography independent of cohesin. Sci Adv 6:eaba8811

Monat C, Padmarasu S, Lux T, Wicker T, Gundlach H, Himmelbach A, Ens J, Li C, Muehlbauer GJ, Schulman AH, Waugh R, Braumann I, Pozniak C, Scholz U, Mayer KFX, Spannagl M, Stein N, Mascher M (2019) TRITEX: chromosome-scale sequence assembly of *Triticeae* genomes with open-source tools. Genome Biol 20:284

Municio C, Antosz W, Grasser KD, Kornobis E, Van Bel M, Eguinoa I, Coppens F, Brautigam A, Lermontova I, Bruckmann A,

Zelkowska K, Houben A, Schubert V (2021) The *Arabidopsis* condensin CAP-D subunits arrange interphase chromatin. New Phytol 230:972–987

Musacchio A, Desai A (2017) A molecular view of kinetochore assembly and function. Biology (Basel) 6:5

Nagaki K, Cheng Z, Ouyang S, Talbert PB, Kim M, Jones KM, Henikoff S, Buell CR, Jiang J (2004) Sequencing of a rice centromere uncovers active genes. Nat Genet 36:138–145

Nechemia-Arbely Y, Fachinetti D, Miga KH, Sekulic N, Soni GV, Kim DH, Wong AK, Lee AY, Nguyen K, Dekker C, Ren B, Black BE, Cleveland DW (2017) Human centromeric CENP-A chromatin is a homotypic, octameric nucleosome at all cell cycle points. J Cell Biol 216:607–621

Němečková A, Wäsch C, Schubert V, Ishii T, Hřibová E, Houben A (2019) CRISPR/Cas9-Based RGEN-ISL allows the simultaneous and specific visualization of proteins, DNA repeats, and sites of DNA replication. Cytogenet Genome Res 159:48–53

Nicklas RB (1965) Chromosome velocity during mitosis as a function of chromosome size and position. J Cell Biol 25:119–135

Nielsen CF, Zhang T, Barisic M, Kalitsis P, Hudson DF (2020) Topoisomerase IIα is essential for maintenance of mitotic chromosome structure. Proc Natl Acad Sci USA 117:12131–12142

Nitiss JL (2009) DNA topoisomerase II and its growing repertoire of biological functions. Nat Rev Cancer 9:327–337

Nozaki T, Imai R, Tanbo M, Nagashima R, Tamura S, Tani T, Joti Y, Tomita M, Hibino K, Kanemaki MT, Wendt KS, Okada Y, Nagai T, Maeshima K (2017) Dynamic organization of chromatin domains revealed by super-resolution live-cell imaging. Mol Cell 67(282-293):e287

Oddone A, Vilanova IV, Tam J, Lakadamyali M (2014) Super-resolution imaging with stochastic single-molecule localization: concepts, technical developments, and biological applications. Microsc Res Tech 77:502–509

Oliveira L, Neumann P, Jang T-S, Klemme S, Schubert V, Koblížková A, Houben A, Macas J (2020) Mitotic spindle attachment to the holocentric chromosomes of *Cuscuta europaea* does not correlate with the distribution of CENH3 chromatin. Front Plant Sci 10:1799

Ono T, Fang Y, Spector DL, Hirano T (2004) Spatial and temporal regulation of condensins I and II in mitotic chromosome assembly in human cells. Mol Biol Cell 15:3296–3308

Palmer DK, O'Day K, Trong HL, Charbonneau H, Margolis RL (1991) Purification of the centromere-specific protein CENP-A and demonstration that it is a distinctive histone. Proc Natl Acad Sci U S A 88:3734–3738

Phengchat R, Hayashida M, Ohmido N, Homeniuk D, Fukui K (2019) 3D observation of chromosome scaffold structure using a 360 degrees electron tomography sample holder. Micron 126:102736

Plačková K, Zedek F, Schubert V, Houben A, Bureš P (2022) Kinetochore size scales with chromosome size in bimodal karyotypes of *Agavoideae*. Ann Bot 130:77–84

Pommier Y, Nussenzweig A, Takeda S, Austin C (2022) Human topoisomerases and their roles in genome stability and organization. Nat Rev Mol Cell Biol 23:407–427

Poonperm R, Takata H, Hamano T, Matsuda A, Uchiyama S, Hiraoka Y, Fukui K (2015) Chromosome scaffold is a double-stranded assembly of scaffold proteins. Sci Rep 5:11916

Poonperm R, Takata H, Uchiyama S, Fukui K (2017) Interdependency and phosphorylation of KIF4 and condensin I are essential for organization of chromosome scaffold. PLoS One 12:e0183298

Ribeiro SA, Vagnarelli P, Dong Y, Hori T, McEwen BF, Fukagawa T, Flors C, Earnshaw WC (2010) A super-resolution map of the vertebrate kinetochore. Proc Natl Acad Sci UA 107:10484–10489

Ryu H, Yoshida MM, Sridharan V, Kumagai A, Dunphy WG, Dasso M, Azuma Y (2015) SUMOylation of the C-terminal domain of DNA topoisomerase IIα regulates the centromeric localization of Claspin. Cell Cycle 14:2777–2784

Samejima K, Samejima I, Vagnarelli P, Ogawa H, Vargiu G, Kelly DA, Alves FD, Kerr A, Green LC, Hudson DF, Ohta S, Cooke CA, Farr CJ, Rappsilber J, Earnshaw WC (2012) Mitotic chromosomes are compacted laterally by KIF4 and condensin and axially by topoisomerase IIα. J Cell Biol 199:755–770

Sanei M, Pickering R, Kumke K, Nasuda S, Houben A (2011) Loss of centromeric histone H3 (CENH3) from centromeres precedes uniparental chromosome elimination in interspecific barley hybrids. Proc Natl Acad Sci U S A 108:E498–E505

Schermelleh L, Ferrand A, Huser T, Eggeling C, Sauer M, Biehlmaier O, Drummen GPC (2019) Super-resolution microscopy demystified. Nat Cell Biol 21(1):72–84

Schittenhelm RB, Althoff F, Heidmann S, Lehner CF (2010) Detrimental incorporation of excess Cenp-A/Cid and Cenp-C into Drosophila centromeres is prevented by limiting amounts of the bridging factor Cal1. J Cell Sci 123:3768–3779

Schroeder-Reiter E, Sanei M, Houben A, Wanner G (2012) Current SEM techniques for de- and re-construction of centromeres to determine 3D CENH3 distribution in barley mitotic chromosomes. J Microsc 246:96–106

Schubert V (2014) RNA polymerase II forms transcription networks in rye and *Arabidopsis* nuclei and its amount increases with endopolyploidy. Cytogenet Genome Res 143:69–77

Schubert V (2017) Super-resolution microscopy – applications in plant cell research. Front Plant Sci 8

Schubert V, Weisshart K (2015) Abundance and distribution of RNA polymerase II in *Arabidopsis* interphase nuclei. J Exp Bot 66:1687–1698

Schubert V, Lermontova I, Schubert I (2014) Loading of the centromeric histone H3 variant during meiosis-how does it differ from mitosis? Chromosoma 123:491–497

Schubert V, Ruban A, Houben A (2016) Chromatin ring formation at plant centromeres. Front Plant Sci 7:28

Schubert V, Neumann P, Marques A, Heckmann S, Macas J, Pedrosa-Harand A, Schubert I, Jang T-S, Houben A (2020) Super-resolution microscopy reveals diversity of plant centromere architecture. Int J Mol Sci 21:3488

Shi W, Tang D, Shen Y, Xue Z, Zhang F, Zhang C, Ren L, Liu C, Du G, Li Y, Yan C, Cheng Z (2019) OsHOP2 regulates the maturation of crossovers by promoting homologous pairing and synapsis in rice meiosis. New Phytol 222:805–819

Shintomi K, Hirano T (2021) Guiding functions of the C-terminal domain of topoisomerase IIα advance mitotic chromosome assembly. Nat Commun 12:2917–2917

Shivanandan A, Deschout H, Scarselli M, Radenovic A (2014) Challenges in quantitative single molecule localization microscopy. FEBS Lett 588:3595–3602

Singh BN, Sopory SK, Reddy MK (2004) Plant DNA topoisomerases: structure, function, and cellular roles in plant development. Crit Rev Plant Sci 23:251–269

Singh BN, Achary VMM, Panditi V, Sopory SK, Reddy MK (2017) Dynamics of tobacco DNA topoisomerases II in cell cycle regulation: to manage topological constrains during replication, transcription and mitotic chromosome condensation and segregation. Plant Mol Biol 94:595–607

Stracy M, Kapanidis AN (2017) Single-molecule and super-resolution imaging of transcription in living bacteria. Methods 120:103–114

Sun M, Biggs R, Hornick J, Marko JF (2018) Condensin controls mitotic chromosome stiffness and stability without forming a structurally contiguous scaffold. Chromosom Res 26:277–295

Talbert PB, Masuelli R, Tyagi AP, Comai L, Henikoff S (2002) Centromeric localization and adaptive evolution of an *Arabidopsis* histone H3 variant. Plant Cell 14:1053–1066

Tichá M, Hlavackova K, Hrbackova M, Ovecka M, Samajova O, Samaj J (2020) Super-resolution imaging of microtubules in Medicago sativa. Methods Cell Biol 160:237–251

Vavrdová T, Šamajová O, Křenek P, Ovečka M, Floková P, Šnaurová R, Šamaj J, Komis G (2019) Multicolour three-dimensional structured illumination microscopy of immunolabeled plant microtubules and associated proteins. Plant Methods 15:22

Vavrdová T, Křenek P, Ovečka M, Šamajová O, Floková P, Illešová P, Šnaurová R, Šamaj J, Komis G (2020) Complementary super-resolution visualization of composite plant microtubule organization and dynamics. Front Plant Sci 11:693

Vos LJ, Famulski JK, Chan GKT (2006) How to build a centromere: from centromeric and pericentromeric chromatin to kinetochore assembly. Biochem Cell Biol 84:619–639

Walther N, Hossain MJ, Politi AZ, Koch B, Kueblbeck M, Odegard-Fougner O, Lampe M, Ellenberg J (2018) A quantitative map of human Condensins provides new insights into mitotic chromosome architecture. J Cell Biol 217:2309–2328

Wang LH, Mayer B, Stemmann O, Nigg EA (2010) Centromere DNA decatenation depends on cohesin removal and is required for mammalian cell division. J Cell Sci 123:806–813

Wang N, Liu J, Ricci WA, Gent JI, Dawe RK (2021) Maize centromeric chromatin scales with changes in genome size. Genetics 217

Wanner G, Schroeder-Reiter E, Ma W, Houben A, Schubert V (2015) The ultrastructure of mono- and holocentric plant centromeres: an immunological investigation by structured illumination microscopy and scanning electron microscopy. Chromosoma 124:503–517

Weisshart K, Fuchs J, Schubert V (2016) Structured illumination microscopy (SIM) and photoactivated localization microscopy (PALM) to analyze the abundance and distribution of RNA polymerase II molecules on flow-sorted Arabidopsis nuclei. Bio Protocol 6:e1725. https://doi.org/10.21769/BioProtoc.1725

Xie L, Dong P, Chen X, Hsieh T-HS, Banala S, De Marzio M, English BP, Qi Y, Jung SK, Kieffer-Kwon K-R, Legant WR, Hansen AS, Schulmann A, Casellas R, Zhang B, Betzig E, Lavis LD, Chang HY, Tjian R, Liu Z (2020) 3D ATAC-PALM: super-resolution imaging of the accessible genome. Nat Methods 17:430–436

Yoon S, Choi E-H, Kim J-W, Kim KP (2018) Structured illumination microscopy imaging reveals localization of replication protein A between chromosome lateral elements during mammalian meiosis. Exp Mol Med 50:112

Yoshida MM, Ting L, Gygi SP, Azuma Y (2016) SUMOylation of DNA topoisomerase IIα regulates histone H3 kinase Haspin and H3 phosphorylation in mitosis. J Cell Biol 213:665–678

Zabka A, Polit JT, Bernasinska J, Maszewski J (2014) DNA topoisomerase II-dependent control of the cell cycle progression in root meristems of *Allium cepa*. Cell Biol Int 38:355–367

Zelkowski M, Zelkowska K, Conrad U, Hesse S, Lermontova I, Marzec M, Meister A, Houben A, Schubert V (2019) *Arabidopsis* NSE4 proteins act in somatic nuclei and meiosis to ensure plant viability and fertility. Front Plant Sci 10:774

Zhang H, Dawe RK (2012) Total centromere size and genome size are strongly correlated in ten grass species. Chromosom Res 20:403–412

Zhang M, Liang C, Chen Q, Yan H, Xu J, Zhao H, Yuan X, Liu J, Lin S, Lu W, Wang F (2020) Histone H2A phosphorylation recruits topoisomerase IIα to centromeres to safeguard genomic stability. EMBO J 39:e101863